Oxygen Fugacity Evolution of the Mantle Lithosphere Beneath the North China Craton

Chen-Yang Ye[1,2], Ji-Feng Ying[1,2,3]*, Yan-Jie Tang[1,2,3], Xin-Miao Zhao[1,3], Hong-Fu Zhang[1,2,3]

[1] State Key Laboratory of Lithospheric Evolution, Institute of Geology and Geophysics, Chinese Academy of Sciences, Beijing 100029, China

[2] College of Earth and Planetary Sciences, University of Chinese Academy of Sciences, Beijing 100049, China

[3] Innovation Academy for Earth Science, Chinese Academy of Sciences, Beijing 100029, China

* Corresponding author: Ji-Feng Ying (email: jfying@mail.iggcas.ac.cn)

ORCID iD: https://orcid.org/0000-0002-1013-8009

Key Words: Oxygen fugacity, Peridotite, Lithospheric mantle, Metasomatism, North China Craton.

Key Points:

- Peridotite xenoliths in Meso-Cenozoic basalts from the North China Craton fall into four groups and record different oxygen fugacities
- The oxygen fugacity variability of the peridotites results from mantle processes associated with the destruction of the North China Craton

Abstract

Oxygen fugacity controls the behavior of multivalent elements and compositions of C-O-H fluids in Earth's mantle, which further affects the cycling of materials between the deep interior and surface of Earth. The redox state of mantle lithosphere of typical stable cratons has been well documented, but how oxygen fugacity had varied during craton destruction remains unclear. This study estimates the oxygen fugacity of peridotite xenoliths entrained in Mesozoic and Cenozoic basalts on North China Craton (NCC), a typical destroyed craton. The results reveal that the mantle lithosphere beneath the NCC experienced three stages of evolution in terms of oxygen fugacity. First, the refractory and oxidized peridotite xenoliths indicate the lithospheric mantle experienced a high degree of melt extraction and later long-term and complicated metasomatism before craton destruction. Then, the variations of olivine Mg-number in peridotites and oxygen fugacity reveal significant metasomatism by melts originated from the shallow asthenosphere during the destruction of the NCC since the Mesozoic. The third stage may have occurred when mantle peridotites interacted with silica-undersaturated melts stemmed from the mantle transition zone where the stagnant Pacific slab underlies. This study further verifies that the asthenospheric convection induced by the roll-back of the subducted paleo-Pacific slab played a crucial role in the destruction of the NCC and helps understand the oxygen fugacity variability during the later life of the craton.

Plain Language Summary

The sub-continental lithospheric mantle is one of the most important reservoirs of carbon. Thus its oxygen fugacity controls the stability of diamond and the compositions of C-O-H fluids. Previous studies have revealed how the oxygen fugacity changes with depth in the upper mantle beneath stable craton. However, cratons are not forever and capable of being destroyed and the North China Craton is one of the most typical destructed cratons globally, as evidenced by extensive magmatism and tectonic deformation since the Mesozoic. The variation of oxygen fugacity during the destruction of the craton, as yet, remains unclear. We estimated the oxygen fugacity of peridotite xenoliths in Mesozoic and Cenozoic basalts on the North China Craton to solve this problem. The oxygen fugacities of the xenoliths record the three-stage evolution of the mantle lithosphere. The evolution process involves complicated secular oxidation before the craton destruction, the widespread reduction by asthenosphere-derived melts, and more oxidized

metasomatism by melts derived from the mantle transition zone, where the subducted Pacific plate is stagnant.

1 Introduction

Oxygen fugacity (f_{O_2}) is a critical parameter that controls the oxidation state of multi-valence elements, such as vanadium, carbon, and iron. (Frost & McCammon, 2008). The variation of f_{O_2} affects the species of C-O-H bearing fluids and melts, which in turn change the solidus and the nature of derived melts (Foley, 2011). For example, as a typical igneous rock that outcropped in stable craton, volatile-rich kimberlites, are generally believed to be the product of interaction between CO_2 and deep upper mantle under an oxidized condition (Sun & Dasgupta, 2020). However, diamond-bearing xenoliths captured by kimberlites imply a reduced background in the lithospheric mantle of the stable craton (Lazarov et al., 2009; McCammon & Kopylova, 2004).

Based on kimberlite-borne peridotite xenoliths, previous studies have established a P-logf_{O_2} profile of stable craton lithospheric mantle (e.g., Creighton et al., 2010; Goncharov et al., 2012; Lazarov et al., 2009). On the one hand, the oxygen fugacity decreases with increasing pressure, proving that diamond is stable in the lower lithospheric mantle (e.g., Creighton et al., 2010; Goncharov et al., 2012; Lazarov et al., 2009). On the other hand, the oxygen fugacity of the stable craton is higher than the ambient asthenosphere, suggesting that oxidized metasomatism may have also influenced the stable craton (Creighton et al., 2009; Foley, 2011).

However, cratons are not forever and capable of being destroyed. The North China craton (NCC) is one of the typical destroyed cratons, as evidenced by extensive magmatism, deformation, and metamorphic core complex during Meso-Cenozoic (Wu et al., 2019). Although numerous studies have been carried out to understand this catastrophic change, the exact cause and detailed mechanism leading to the craton destruction is still hotly debated. Primarily, few investigations are from a perspective of mantle redox state. So, it is valuable to figure out the redox state of the upper mantle beneath the NCC at different geological times, how oxygen fugacity varied and clues that f_{O_2} of peridotite xenoliths bears to unravel the geological processes during the craton destruction.

This paper collects numerous published geochemical data of peridotite xenoliths entrained in Mesozoic and Cenozoic basalts on North China Craton (NCC) and estimates their oxygen

fugacity. The yielded data reveal the redox state of the mantle lithosphere beneath the NCC and how it has changed during the craton destruction and factors affecting such variations.

2 Geological Setting

The NCC is one of the oldest cratons in the world with Archean crustal remnants as old as 3.8 Ga (Liu et al., 1992). It can be divided into the Eastern Block, the Trans-North China Orogen (TNCO), and the Western Block based on geology, tectonic evolution, and P–T–t paths of metamorphic basement rocks (Figure 1) (Zhao et al., 2005). It is generally reckoned that the Eastern and Western blocks evolved independently from late Archean to early Paleoproterozoic times before colliding into a coherent craton and final cratonization along the Trans-North China Orogen belt at ca. 1.85 Ga (Zhao et al., 2005). Since then, the NCC had essentially remained stable until the Mesozoic.

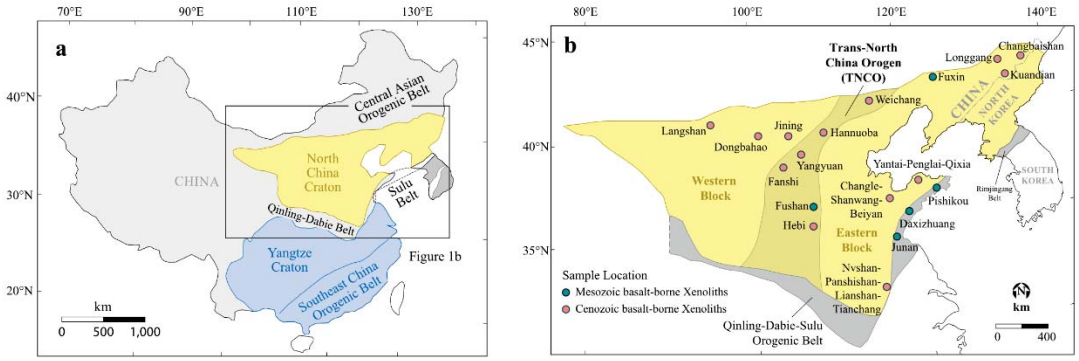

Figure 1. (a) Tectonic subdivision of the Chinese continent and the location of the NCC (modified after Wu et al., 2019). (b) Schematic geological map of the NCC, showing the three-fold tectonic subdivision (modified after Wu et al., 2019) and the localities of peridotites xenoliths entrained by Mesozoic and Cenozoic mafic rocks.

Since the Mesozoic, deformation and extensive magmatism triggered by circum-craton subduction suggest the NCC, except the Western Block, has lost its stability (Wu et al., 2019). From the view of peridotite xenoliths, the thick refractory lithospheric keel was removed and replaced by fertile peridotites (Zheng et al., 2012). Meanwhile, the geotherm of the lithosphere underneath the eastern part of the NCC soared from 40 mW/m2 in Paleozoic to >80 mW/m^2 in Mesozoic (Menzies & Xu, 1998). Likewise, geophysical imagining verifies that the thickness of the lithosphere of the Eastern Block is drastically thinned to about 70-80 km from greater than

200 km in Paleozoic. In contrast, the Western Block keeps almost intact (Chen et al., 2009). Accompanied by the NCC destruction are the widespread Meso-Cenozoic basaltic rocks, especially in the Eastern Block and the TNCO, which captured a large amount of mantle peridotite xenoliths. Previous investigations on these xenoliths have yielded an enormous amount of geochemical data, making it possible to draw a whole picture of the redox state of the mantle lithosphere beneath the NCC.

3 Data, or a descriptive heading about data

Thanks to previous studies, ample mineral compositions of peridotite xenoliths entrained in both Mesozoic and Cenozoic basalts are available to date, which gives us an excellent chance to do the research comprehensively. All the available peridotite xenoliths captured by basalts of different ages and locations are all compiled in Figure 1. After collecting 605 peridotite xenoliths, we estimate each sample's equilibrium temperature and oxygen fugacity before performing subsequent statistical analysis. The reference of each sample is listed in Text S1.

The abovementioned peridotite xenoliths are mainly harzburgite and lherzolite, with a few amounts of wehrlite (Figure 2). We divide them into four groups based on the modal abundance and the Mg-number of olivine. The first group consists of Fushan, Hebi, and other localities from the Western Block of the NCC. The first group consists of Fushan, Hebi, and other localities from the Western Block of the NCC. The first-group xenoliths likely represent the relics of the Archean mantle due to their high olivine modal abundance and Mg-number (Figure 3a), and the Archean ages revealed by osmium isotope (Liu et al., 2011; Xu et al., 2010; Zheng et al., 2001). Geophysical imaging has demonstrated that the lithosphere of the Western Block underwent insignificant thinning (Chen et al., 2009). Therefore, peridotites xenoliths from the Western Block can also represent the ancient lithospheric mantle. However, the mineral modal abundance and chemical composition are somewhat different from those of Fushan and Hebi. The second group of xenoliths are relatively high in olivine modal abundance and Mg-number and fall into the Proterozoic field (Figure 3b). Thus, we name them "High-Mg Peridotites". The third group samples belong to "Low-Mg Peridotites" due to their lower modal abundance and Mg-number of olivine relative to the High-Mg ones. They follow the oceanic trend proposed by Boyd (1989) and dominantly fall into the Phanerozoic field (Figure 3c). As for the fourth group, the Mg-

number of olivine is lower than 88, with the lowest value being as low as 80 (Figure 3d), which differs sharply from that of the sub-continental lithospheric mantle (Griffin et al., 1999). Hence, we call them "Anomalously Low-Mg Peridotite". Among these xenoliths, "Low-Mg Peridotites" and "High-Mg Peridotites" dominate our samples (~53% and ~28% respectively), while the first group and the fourth group take ~12% and 7% of the samples, respectively. We perform discriminant analysis for those without published modal abundance data to judge whether they belong to the "High-Mg" or "Low-Mg". In our case, the Mg-number of olivine equal to 90.5 as the group discrimination criteria is feasible. The peridotites whose olivine have Mg-number higher than 90.5 belong to "High-Mg Peridotites". In contrast, those with olivine Mg-number between 88~90.5 belong to "Low-Mg Peridotites".

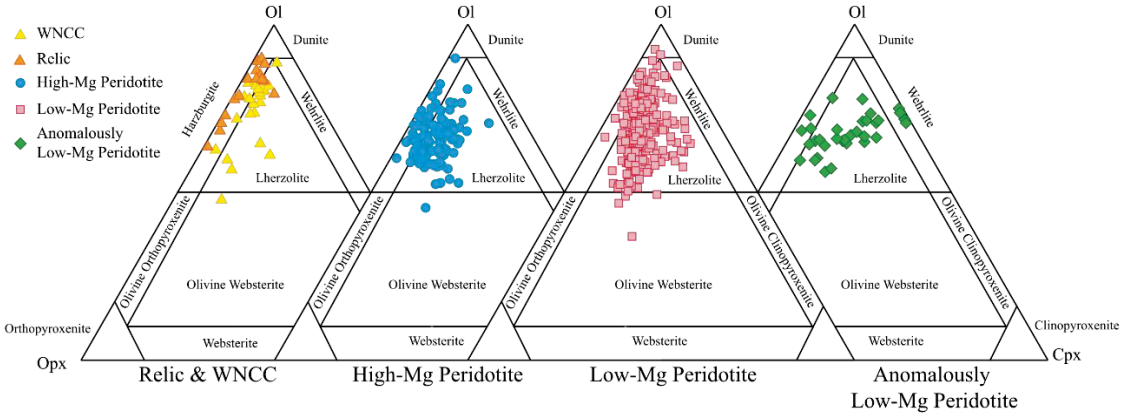

Figure 2. Petrological classification for peridotite xenoliths from the North China Craton (The detailed data are listed in **Table S1**). The brown and yellow triangle, circle, square, and diamond symbols represent the relics and those from the western NCC (WNCC), high-Mg, low-Mg, and anomalously low-Mg samples, respectively. The scheme for grouping is based on the Mg-number and modal abundance of olivine in each sample. Samples having olivine less than 50% are excluded.

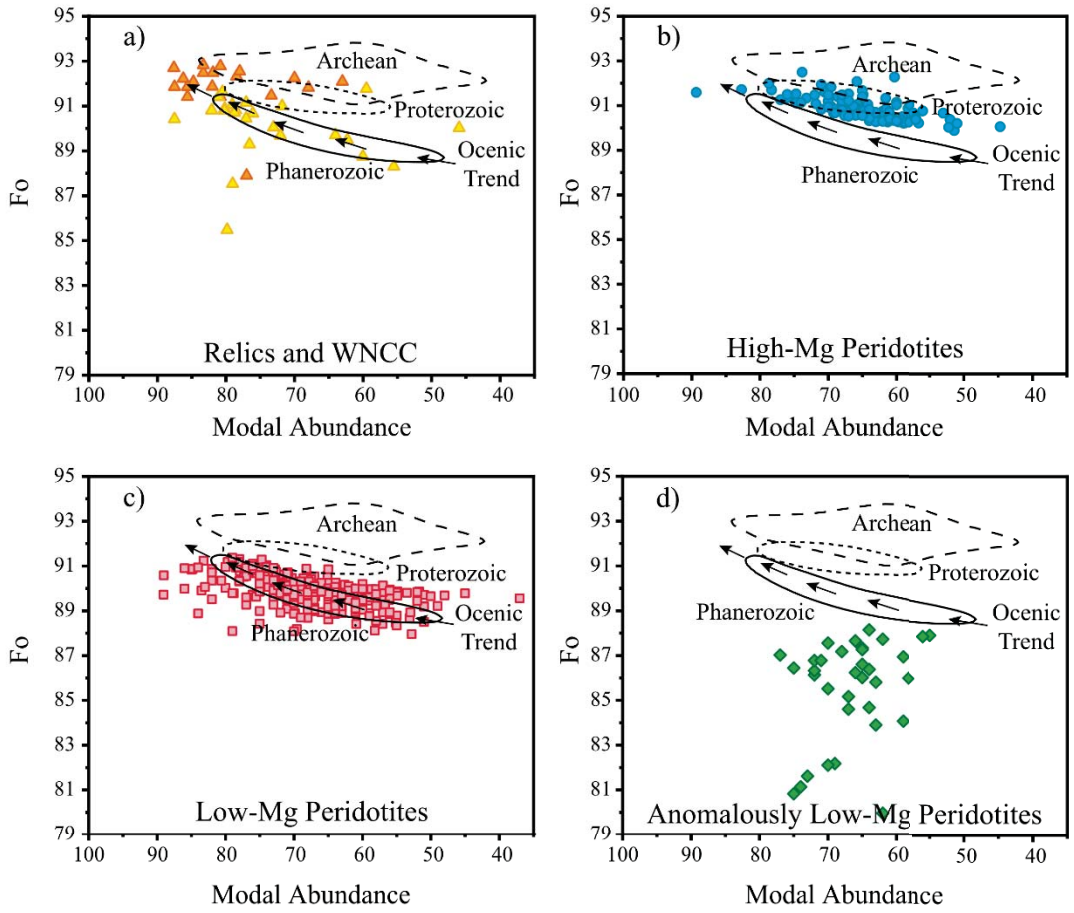

Figure 3. Olivine Mg-number vs. modal abundance for peridotite xenoliths from the North China Craton (The detailed data are listed in **Table S1**). The oceanic trend is after Boyd (1989). The Archean, Proterozoic, and Phanerozoic fields are from Griffin et al. (1999). Symbols are the same as in Figure 2.

4 Methods and Results

Since all samples compiled are spinel-facies peridotites, there are no suitable geobarometers that can be used to yield reasonable pressure estimation to date. Therefore, we assume an equilibrium pressure of 1.5 GPa for subsequent calculations of temperature and oxygen fugacity.

4.1 Equilibrium Temperature

Many geothermometers have been calibrated to date, but not all are applicable in our study, primarily because lacking raw data for the calculation of key parameters. Therefore, we choose the two-pyroxene thermometers (Brey & Kohler, 1990; Taylor, 1998) or the enstatite-in-Cpx

thermometer (Nimis & Taylor, 2000) to estimate the equilibrium temperatures of these xenoliths. For samples that are Cpx-poor or devoid of chemical compositions of Cpx, their equilibrium temperatures are calculated based on the Ol-Sp thermometer (Coogan et al., 2014).

As all above mentioned pyroxene-related thermometers are developed based on the similar enstatite-exchange between Opx and Cpx (Nimis & Gruetter, 2010), they yield nearly consistent outcomes within errors (Table S2). By contrast, the Ol-Sp thermometer usually gives slightly higher temperatures (Table S2).

The statistical results show that no matter where the peridotites are from or which group the xenoliths belong to, they all have similar temperatures (Table 1). Compared with those from the other tectonic units of the NCC, peridotites from the Trans-North China Orogen (TNCO) appear more homogeneous in temperature. Furthermore, if we project the average temperature to the geotherm of North China Craton in Mesozoic (> 80mW/m^2), an estimation of ~1.5 GPa can be inferred, confirming the reasonability of our assumption of an equilibrium pressure of 1.5 GPa for these xenoliths.

4.2 Oxygen Fugacity

Oxygen fugacity of spinel-facies peridotites is recorded by the thermodynamic equilibrium of Olivine-Orthopyroxene-Spinel assemblages (O'Neill & Wall, 1987):

$$\underset{Ol}{6Fe_2SiO_4} + O_2 \leftrightarrow \underset{Opx}{3Fe_2Si_2O_6} + \underset{Sp}{2Fe_3O_4} \quad (1)$$

Previous experiments have proposed two types of oxybarometers, one of which relies on the activity of Fe_3O_4 (e.g., Davis et al., 2017; Mattioli & Wood, 1988) and another requires $Fe^{3+}/\sum Fe$ by calculation assuming perfect stoichiometry (Ballhaus et al., 1991). Compared with the former equation, the advantage of the latter is that it directly links f_{O_2} to mineral compositions analyzed by EPMA, especially when Mössbauer spectroscopy is unavailable, and thus avoids correction of spinel and errors introduced during the calculating activity of magnetite end-member. Therefore, we choose the equation proposed by Ballhaus et al. (1991) to estimate the f_{O_2}.

The calculated oxygen fugacities of the peridotite xenoliths are shown in Figure 4 and Table 2 and S2. The Ni precipitation curve reaches nearly FMQ-4 under 1.5 GPa (Frost & McCammon, 2008; O'Neill & Wall, 1987), implying the appearance of Ni-bearing peridotite. Nevertheless, no Ni-bearing peridotites are reported on the NCC yet. Therefore, samples with f_{O_2} lower than FMQ-4 are excluded for further discussion. The results show that for peridotites falling into SCLM fields, f_{O_2} decreases along with lowering Mg-number (Figure 4). However, the "Anomalously Low-Mg Peridotites" have relatively higher f_{O_2}, which is between the "High-Mg Peridotites" and peridotites being regarded as Archean relics and from the Western Block (Figure 4).

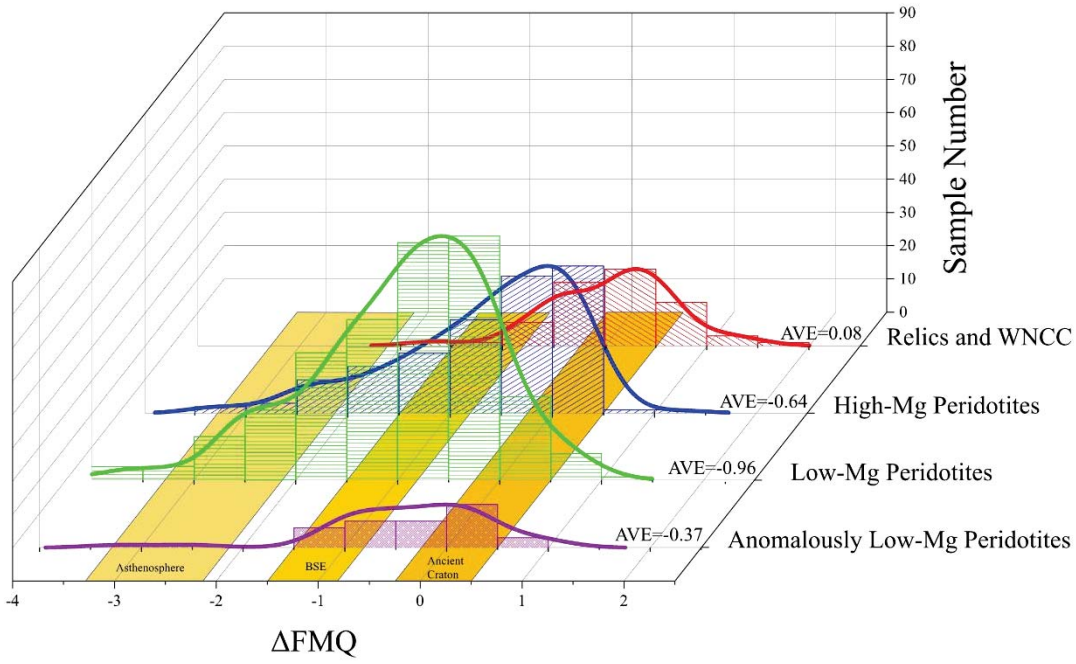

Figure 4. The oxygen fugacity of peridotites from the North China Craton. The grouping scheme follows that in Figure 3. The data of each group shows in the form of the histogram and corresponding kernel density estimation (**the detailed data are listed in Table S2**). The oxygen fugacity of the ancient craton is extrapolated from other stable cratons (Slave Craton: Creighton et al., 2010, McCammon and Kopylova, 2004; Siberia Craton: Goncharov et al., 2012, Yaxley et al., 2012; Kaapvaal Craton: Lazarov et al., 2009, Woodland and Koch, 2003) to 1~2 Gpa, under which only spinel-facies peridotites are stable. The oxygen fugacity between 1~2 GPa of the Bulk Silicate Earth (BSE) mantle is calculated via methods proposed by Stagno et al. (2013). As the Fe_2O_3 content of the asthenosphere ranges between 0.3 and 0.5 wt% (Cottrell & Kelley, 2011;

208 Sorbadere et al., 2018) and the primary melts record the same f_{O_2} to the equilibrated residues
209 (Birner et al., 2018; Davis & Cottrell, 2018), we estimate the oxygen fugacity of hypothetical
210 melts identical to the composition of the asthenosphere under 1~2 GPa and 950 ℃. The average
211 oxygen fugacity of the normal mantle decreases with decreasing Mg-number of olivine.
212 However, the anomalously low-Mg peridotites are slightly more oxidized than the high-Mg and
213 low-Mg ones.

214

215 **Table 1.** Temperature estimations for peridotites from the North China Craton (the detailed data are listed in **Table S2**)

Group	Archean relics (n=47)	WNCC (n=21)	High-Mg			Low-Mg			Anomalously Low-Mg		
			TNCO (n=82)	ENCC (n=80)	Total (n=162)	TNCO (n=101)	ENCC (n=205)	Total (n=306)	TNCO (n=10)	ENCC (n=30)	Total (n=40)
Temperature (°C)	951.68	882.43	973.93	923.93	949.24	952.73	939.05	943.56	1031.69	948.36	969.19
S.D.	150.52	109.00	86.62	132.25	114.28	84.74	127.66	115.45	74.44	108.37	107.22

216

217 **Table 2.** Oxygen fugacity estimations for peridotites from the North China Craton (the detailed data are listed in **Table S2**)

Group	Archean relics (n=47)	WNCC (n=21)	High-Mg			Low-Mg			Anomalously Low-Mg		
			TNCO (n=82)	ENCC (n=80)	Total (n=162)	TNCO (n=101)	ENCC (n=205)	Total (n=306)	TNCO (n=10)	ENCC (n=30)	Total (n=40)
ΔFMQ	0.13	-0.07	-0.61	-0.67	-0.64	-1.01	-0.93	-0.96	-0.17	-0.43	-0.37
S.D.	0.59	0.64	0.83	0.91	0.87	0.93	0.89	0.90	0.87	0.77	0.80

5 Discussion

5.1 Oxygen fugacity of cratonic mantle

Before discussing how f_{O_2} of lithospheric mantle evolved during craton destruction, it is crucial to test if the peridotites of Archean relics and those from the Western Block can be treated as starting points, namely, whether their f_{O_2} resemble that of typical stable cratonic mantle lithosphere. As previous studies mainly focused on kimberlite-borne garnet-facies peridotites rather than spinel-facies ones (e.g., Lazarov et al., 2009; Woodland & Koch, 2003; Yaxley et al., 2012), to extrapolate P- logf_{O_2} curves to 1~2 Gpa, under which spinel-facies peridotites are stable (e.g., Till et al., 2012; Ziberna et al., 2013) is a prerequisite. In theory, when coexisting spinel and garnet reach thermodynamic equilibrium, they record consistent oxygen fugacity (Miller et al., 2016). Besides, studies of Siberia Craton also support that pressure and f_{O_2} of spinel-facies and garnet-facies peridotites fit well in the same curve (Goncharov et al., 2012). McCammon and Kopylova (2004) found more reduced spinel peridotites that deviate from the P-logf_{O_2} curve in Slave Craton. Notwithstanding, this is usually interpreted to be the result of a high degree of depletion. Therefore, the extrapolation of f_{O_2} of mantle lithosphere from garnet to spinel facies is reasonable and appropriate.

Extrapolation of P-logf_{O_2} that combined data from Slave Craton, Siberia Craton, and Kaapvaal Craton follows the equation (Figure 5):

$$\Delta FMQ=1.37-0.86*P \qquad (2)$$

The gradient of the P-logf_{O_2} is similar to those reported in previous studies (Slave Craton: -0.59 log/GPa, McCammon and Kopylova, 2004; Siberia Craton: -0.83 log/GPa, Goncharov et al., 2012; -1.0 log/GPa, Yaxley et al., 2012; Kaapvaal Craton: -1.0 log/GPa, Lazarov et al., 2009; and -0.86 log/GPa, Woodland and Koch, 2003). Under 1~2 GPa, the extrapolation of stable cratons' P-logf_{O_2} curve is nearly consistent with the oxygen fugacity of the first group samples, which represent relics

of the Archean lithospheric mantle (Figure 4). Thus, we propose that peridotites of the first group reflect the redox state of the mantle lithosphere before the destruction of the NCC. Furthermore, similar to typical stable craton around the world, peridotites from the first group have higher f_{O_2}, which could be the outcome of oxidized, sometimes multi-stage metasomatism, as evidenced by trace elements and in-situ Sr isotope of clinopyroxene (Creighton et al., 2010; Creighton et al., 2009; Dai et al., 2019; Wu et al., 2017; Xu et al., 2010; Zheng et al., 2001).

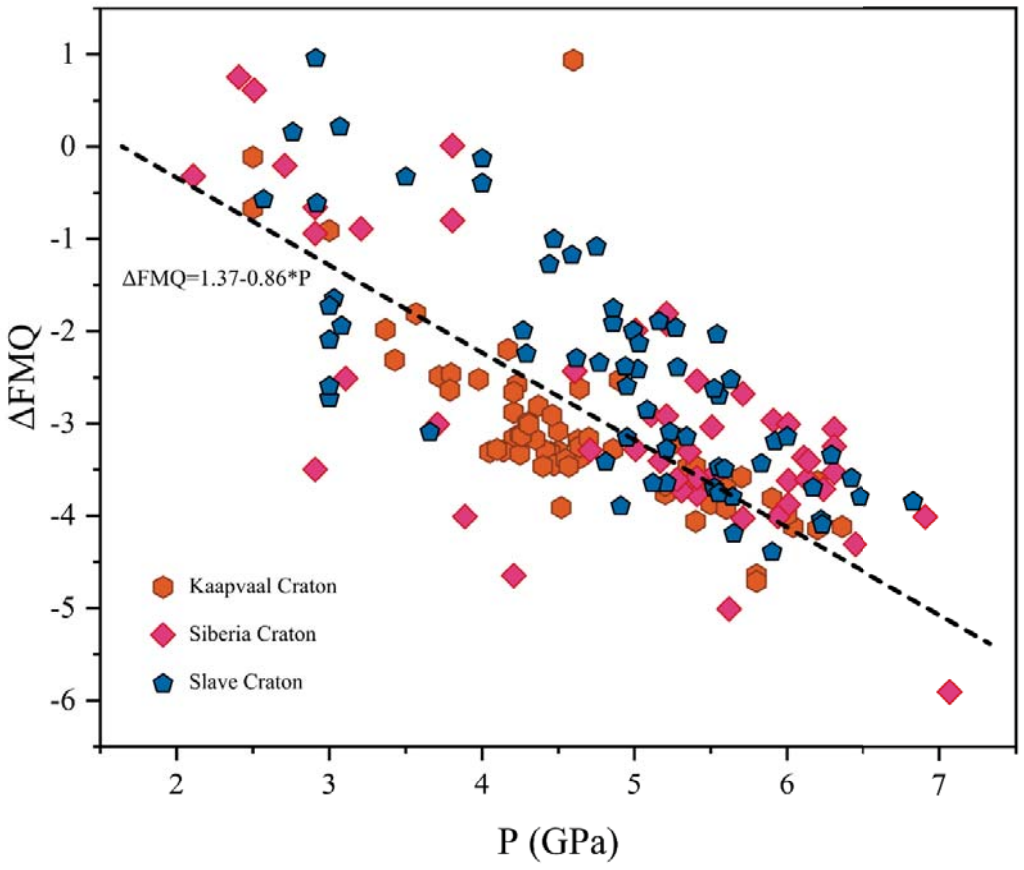

Figure 5. Correlation between the oxygen fugacity and equilibrium pressure of peridotites from Kaapvaal Craton, Siberia Craton, and Slave Craton. The dashed line fitting these data serves for the oxygen fugacity extrapolation from garnet facies to spinel facies mantle. Data source: Kaapvaal Craton: Lazarov et al. (2009), Woodland and Koch (2003); Siberia Craton: Goncharov et al. (2012), Yaxley et al. (2012); Slave Craton: Creighton et al. (2010), McCammon and Kopylova (2004) (the detailed data are listed in **Table S3**).

5.2 Variation of oxygen fugacity during craton destruction

Craton destruction resulted from the removal or replacement of the ancient refractory lithospheric keels by fertile materials (Tang et al., 2008; Xiao et al., 2010; Ying et al., 2006), which is also clearly demonstrated by our observation as more than 50% of samples fall into Phanerozoic fields (Figure 3). Along with craton destruction, the oxygen fugacity of peridotites tends to be more reduced (Figure 4). Potential mechanisms leading to the reduction of lithospheric mantle include: 1) a higher degree of melt extraction (Gaillard et al., 2015), 2) metasomatism by reduced fluids (Griffin et al., 2018), and 3) metasomatism by reduced melts (Creighton et al., 2010; Goncharov et al., 2012).

In theory, the higher degree of melt extraction the mantle peridotites suffer, the lower $\boldsymbol{f_{O_2}}$ the peridotite residues will record (Gaillard et al., 2015). However, the studied samples with a lower degree of melt extraction, as reflected by low Mg-numbers, commonly have lower oxygen fugacity (Figure 4), indicating that partial melting cannot account for the reduction during craton destruction.

When reduced fluids (mainly CH_4+H_2O) interact with the ambient mantle, methane can be oxidized to diamond (e.g., Smit et al., 2016; Thomassot et al., 2007), and the lithospheric mantle will get reduced correspondingly (Griffin et al., 2018). However, three lines of evidence argue against that CH_4+H_2O fluids reduced the mantle lithosphere underneath the NCC. First, under the circumstance of ~950 °C and 1.5 GPa, only when $\boldsymbol{f_{O_2}}$ is lower than FMQ-3.25, the dominant species in the fluids is CH_4 (Figure 6). By contrast, the $\boldsymbol{f_{O_2}}$ of most peridotites from the NCC are above FMQ-2 with only minor equilibrating with CH_4-dominated fluids (Figure 4). Furthermore, if fluids and peridotites had reached an equilibrium, what can be predicted is that the proportion of water caused by the oxidation of methane will increase with increasing $\boldsymbol{f_{O_2}}$, which will likely lead to an increase of water content in peridotite. However, no such correlation exists in our dataset (Figure 7). Moreover, the interaction of the mantle peridotites with reduced fluids would produce materials

that reflect reduced conditions, such as diamond, SiC, and metal-alloy (Griffin et al., 2018). However, no such materials havebeen reported yet in peridotites entrained by Mesozoic and Cenozoic mafic rocks. Therefore, we argue that reduced fluids are highly unlikely to be the primary driving force reducing the mantle.

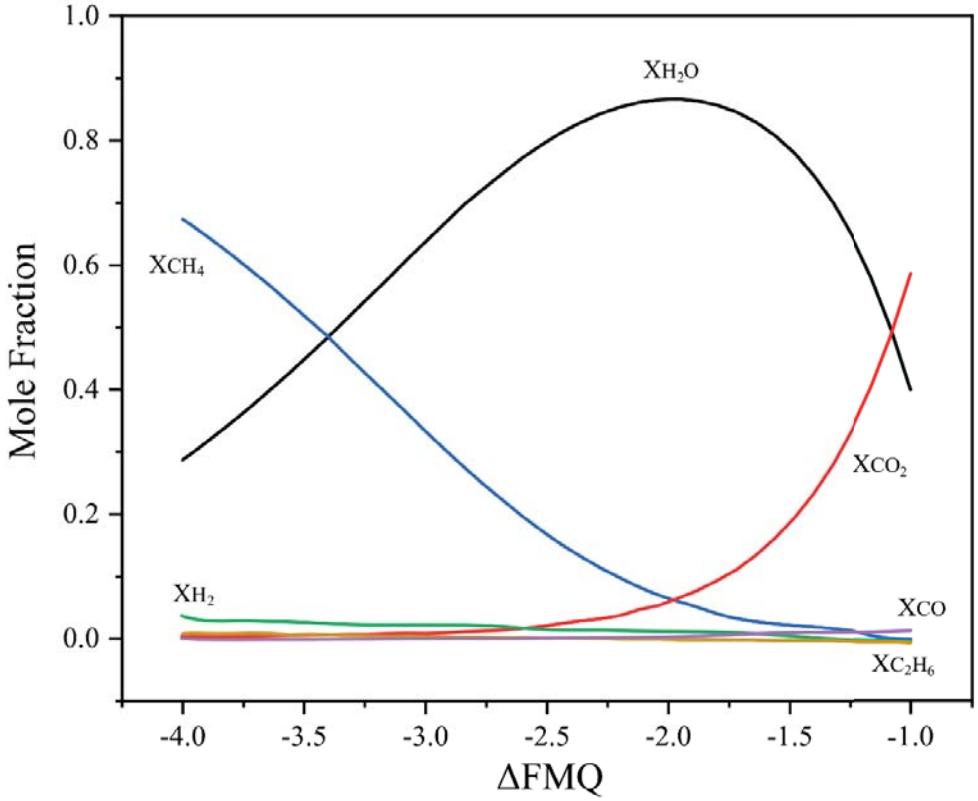

Figure 6. Variation of fluids species vs. oxygen fugacity under 950 ℃ and 1.5 GPa. The composition of fluids is calculated via GFluid (Zhang & Duan, 2009, 2010; The detailed data are listed in **Table S4**). The proportion of CH_4 increases with decreasing f_{O_2}, while CO_2 decreases with decreasing f_{O_2}. With lowering f_{O_2}, the proportion of H_2O rises and reaches the peak at ΔFMQ=-2 at first and then declines. When f_{O_2} reaches ΔFMQ=-3.46, the fractions of CH_4 and H_2O are identical. Other minor species (H_2, CO, and C_2H_6) show negligible variation.

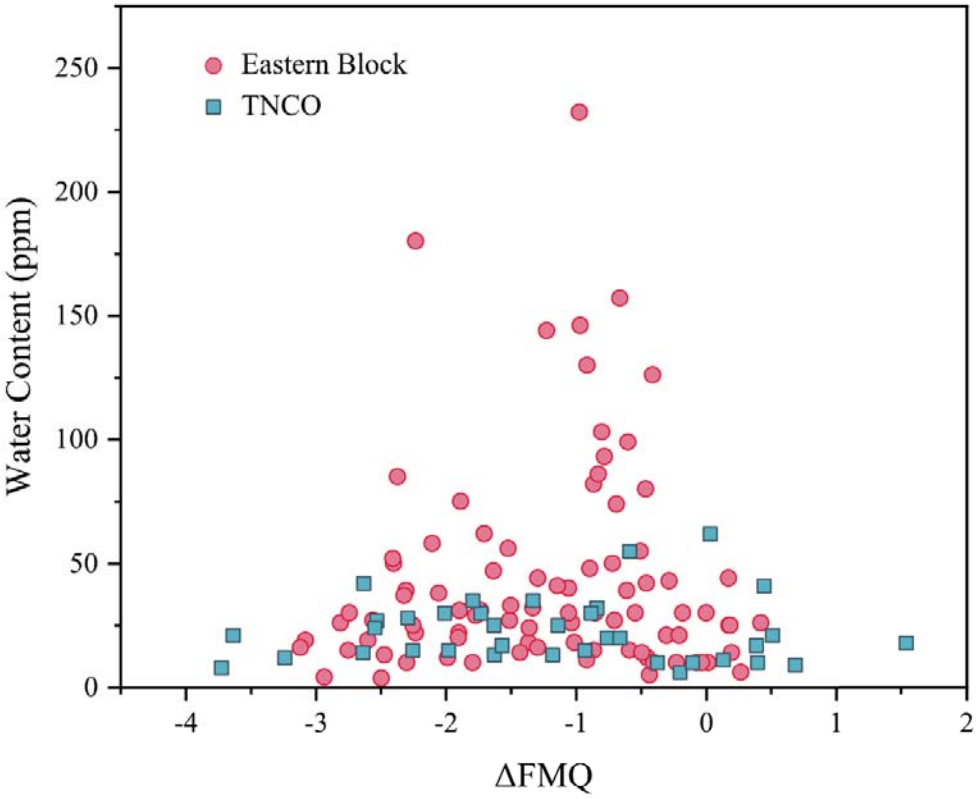

Figure 7. Whole-rock water content vs. the oxygen fugacity of peridotite from the North China Craton. Both peridotites from the Trans-North China Orogen (TNCO) and the Eastern Block (EB) show no correlation between water content and f_{O_2}. Data source: Hao et al. (2016), Li et al. (2015), Wang et al. (2014), Xia et al. (2010), Xia et al. (2013), Yang et al. (2008). The detailed data are listed in **Table S5.**

5.3 Origin of the Anomalously Low-Mg Peridotite

Some samples from Yangyuan, Beiyan, Fuxin, Daxizhuang, and Longgang have very low Mg-number (generally lower than 88), inconsistent with a typical craton mantle. They are higher in $\boldsymbol{f_{O_2}}$ than all other peridotites but those of the first group (Figure 4). Therefore, an alternative process rather than metasomatism by asthenospheric materials is required to account for this anomaly.

Wehrlite and Cpx-rich lherzolite are preponderant in the Anomalously Low-Mg Peridotite group (Figure 2). Two modes of origin have been proposed for wehrlite,

including mafic-ultramafic cumulate (e.g., Mattielli et al., 1996) and product of metasomatism (e.g., Gervasoni et al., 2017; Ionov et al., 2005). The wehrlite studied here cannot be mafic-ultramafic cumulate because they have no cumulate texture. Experiments have demonstrated that Opx-poor lherzolite and wehrlite could result from the interaction between rock and silica-undersaturated basaltic melts or silicate-carbonate melts. The peridotite-melt reaction could dissolve orthopyroxene while generating olivine and clinopyroxene (Gervasoni et al., 2017; Kelemen et al., 1990). This interpretation is reasonable because silica-undersaturated alkali basalts, which are also oxidized, outcrop extensively on the NCC after ~100 Ma (Hong et al., 2020; Li et al., 2017). More convincingly, Zhang et al. (2007) reported a hand-specimen scale phenomenon that a wehrlite rim formed between a lherzolite and its host alkali basalt. Therefore, the metasomatism of silica-undersaturated melts could lower the Mg-number but raise the oxygen fugacity of the peridotites.

5.4 Tectonics implication

Peridotites have weak buffer capacity, implying their oxygen fugacity is easily reset and thus only record the influence of the last metasomatism (Luth & Stachel, 2014). From the view of f_{O_2}, different groups of spinel-facies peridotites from the NCC jointly record multi-stage metasomatism during its evolution.

The first stage of evolution (Figure 8a), corresponding to the time period since the final cratonization of the NCC and before the craton destruction, is recorded by the first group of peridotites. Their higher Mg-number of olivine and f_{O_2} are similar to those of typical stable craton (Goncharov et al., 2012), implying a high degree of melt extraction and subsequent oxidized metasomatism by fluids or melts that might be released during the amalgamation of the Eastern and Western Block at ca. 1.85 Ga.

The second stage of evolution is craton destruction (Figure 8b~e). The relics, High-Mg, and Low-Mg peridotites, primarily record the interaction between the asthenosphere and shallow craton lithospheric mantle, with minor direct accretion of

the asthenosphere. Multiple subductions, especially the Paleo-Pacific subduction and subsequent slab roll-back, eroded the above lithosphere, facilitating upwelling melts' infiltration and creating chemically weak zones (Foley, 2008; Wu et al., 2019). In addition, the Tan-Lu fault zone, a lithosphere deep fault, also facilitates the development of a physically weak zone (Xiao et al., 2010). Therefore, along with the slab roll-back, the asthenosphere laterally convected to the base of the lithosphere and then infiltrated and interacted with the shallow lithospheric mantle (Zheng et al., 2018), resulting in the observed trend that f_{O_2} decreases with decreasing Mg-number of olivine. The ancient lithospheric mantle loses its stability after being eroded or even dismembered by the asthenosphere, which led to the destruction of the NCC.

The third stage of evolution is not a ubiquitous phenomenon and probably a locally occurred process (Figure 8e). The lowering of Mg-number of olivine with increasing f_{O_2} is likely attributed to the metasomatism by silica-undersaturated basaltic melts. Silica-undersaturated basaltic melts that host and interact with xenoliths could originate from the deep upper mantle metasomatized by melts from the stagnant Pacific slab (Xu et al., 2018). The asthenosphere was involved in the metasomatism of both the second and the third stages. However, the source depth of the metasomatic agents ultimately determined the different outcomes. The shallow asthenosphere could not have been oxidized by melts derived from the stagnant slabs, whereas the deep part has. This phenomenon justifies the mantle lithosphere's vertical heterogeneity (Xu et al., 2018). Moreover, the f_{O_2} profile of a reduced shallow and an oxidized deep upper mantle of the NCC is in sharp contrast to typical stable cratons.

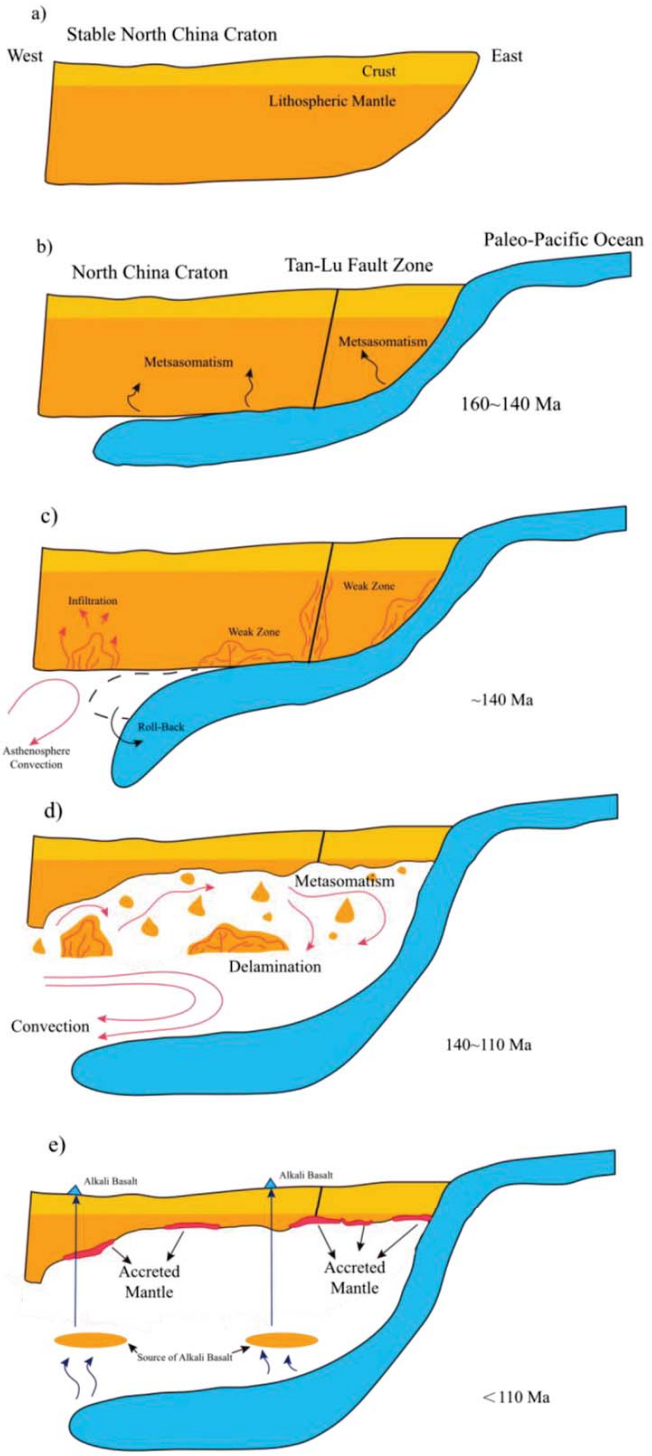

Figure 8. Schematic tectonic evolution of the North China Craton (not in scale). (a) Fluids and melts derived from adjacent plates oxidized the NCC lithospheric mantle before craton destruction. (b) Fluids released by flat subduction of the Paleo-Pacific metasomatized and weakened the lithospheric mantle. (c) The subducted plate rolled

back, inducing mantle convection, and weak zones facilitated the infiltration of the asthenospheric melts. (d) Intensive asthenosphere convection dismembered the lithospheric mantle with erosion and local delamination. (e) Metasomatism of asthenosphere-derived melt lowered the oxygen fugacity of the mantle lithosphere, associated with minor accretion. During the Cenozoic, silica-unsaturated melts from the mantle metasomatized by stagnant slab interacted with xenoliths, forming the Cpx-rich lherzolites and wehrlites.

6 Conclusions

1. Peridotite xenoliths captured by Meso-Cenozoic basalts on the NCC record the variation of oxygen fugacities in the mantle lithosphere beneath the destroyed craton.

2. Peridotite xenoliths from the Western Block of the NCC are relics of the Archean mantle and representative of the mantle lithosphere before the craton destruction. Their high f_{O_2} could result from the long-term and complicated metasomatism since its cratonization and before the craton destruction.

3. A trend displayed by the majority of peridotite xenoliths of lowering f_{O_2} with decreasing Mg-number of olivine might have resulted from extensive metasomatism by melts derived from shallow asthenosphere, rather than melt extraction or metasomatism by reduced fluids.

4. The Anomalously Low-Mg Peridotites exhibit higher f_{O_2} relative to those of the Low-Mg Peridotites, suggesting that the former are probably the products of metasomatism by silica-undersaturated basaltic melts derived from deep asthenosphere, impinged by melts from the stagnant Pacific slab.

Acknowledgments

This work was financially supported by the National Natural Science Foundation of China (Grant Nos. 41688103, 41725014). The authors declare that they have no competing interests. All data supporting the conclusions of this paper can be found in

the cited references, tables, and supporting information. These data are also accessible in Mendeley data https://data.mendeley.com/datasets/k5nvgspkmf/draft?a=3863ec55-0280-49f0-9f39-8b5d2c2e7fd9.Any real or perceived financial conflicts of interests for any author

References

Ballhaus, C., Berry, R. F., & Green, D. H. (1991). High-pressure experimental calibration of the olivine-ortho-pyroxene-spinel oxygen geobarometer - implications for the oxidation-state of the upper mantle. *Contributions to Mineralogy and Petrology, 107*(1), 27-40. doi:10.1007/bf00311183

Birner, S. K., Cottrell, E., Warren, J. M., Kelley, K. A., & Davis, F. A. (2018). Peridotites and basalts reveal broad congruence between two independent records of mantle f(O2) despite local redox heterogeneity. *Earth and Planetary Science Letters, 494*, 172-189. doi:10.1016/j.epsl.2018.04.035

Boyd, F. R. (1989). Compositional distinction between oceanic and cratonic lithosphere. *Earth and Planetary Science Letters, 96*(1-2), 15-26. doi:10.1016/0012-821x(89)90120-9

Brey, G. P., & Kohler, T. (1990). Geothermobarometry in 4-phase lherzolites .2. new thermobarometers, and practical assessment of existing thermobarometers. *Journal of Petrology, 31*(6), 1353-1378. doi:10.1093/petrology/31.6.1353

Canil, D., & O'Neill, H. S. C. (1996). Distribution of ferric iron in some upper-mantle assemblages. *Journal of Petrology, 37*(3), 609-635. doi:10.1093/petrology/37.3.609

Chen, L., Cheng, C., & Wei, Z. (2009). Seismic evidence for significant lateral variations in lithospheric thickness beneath the central and western North China Craton. *Earth and Planetary Science Letters, 286*(1-2), 171-183. doi:10.1016/j.epsl.2009.06.022

Coogan, L. A., Saunders, A. D., & Wilson, R. N. (2014). Aluminum-in-olivine

thermometry of primitive basalts: Evidence of an anomalously hot mantle source for large igneous provinces. *Chemical Geology, 368*, 1-10. doi:10.1016/j.chemgeo.2014.01.004

Cottrell, E., & Kelley, K. A. (2011). The oxidation state of Fe in MORB glasses and the oxygen fugacity of the upper mantle. *Earth and Planetary Science Letters, 305*(3-4), 270-282. doi:10.1016/j.epsl.2011.03.014

Creighton, S., Stachel, T., Eichenberg, D., & Luth, R. W. (2010). Oxidation state of the lithospheric mantle beneath Diavik diamond mine, central Slave craton, NWT, Canada. *Contributions to Mineralogy and Petrology, 159*(5), 645-657. doi:10.1007/s00410-009-0446-x

Creighton, S., Stachel, T., Matveev, S., Hoefer, H., McCammon, C., & Luth, R. W. (2009). Oxidation of the Kaapvaal lithospheric mantle driven by metasomatism. *Contributions to Mineralogy and Petrology, 157*(4), 491-504. doi:10.1007/s00410-008-0348-3

Dai, H.-K., Zheng, J.-P., Xiong, Q., Su, Y.-P., Pan, S.-K., Ping, X.-Q., & Zhou, X. (2019). Fertile lithospheric mantle underlying ancient continental crust beneath the northwestern North China craton: Significant effect from the southward subduction of the Paleo-Asian Ocean. *Geological Society of America Bulletin, 131*(1-2), 3-20. doi:10.1130/b31871.1

Davis, F. A., & Cottrell, E. (2018). Experimental investigation of basalt and peridotite oxybarometers: Implications for spinel thermodynamic models and Fe^{3+} compatibility during generation of upper mantle melts. *American Mineralogist, 103*(7), 1056-1067. doi:10.2138/am-2018-6280

Davis, F. A., Cottrell, E., Birner, S. K., Warren, J. M., & Lopez, O. G. (2017). Revisiting the electron microprobe method of spinel-olivine-orthopyroxene oxybarometry applied to spinel peridotites. *American Mineralogist, 102*(1-2), 421-435. doi:10.2138/am-2017-5823

Foley, S. F. (2008). Rejuvenation and erosion of the cratonic lithosphere. *Nature*

Geoscience, 1(8), 503-510. doi:10.1038/ngeo261

Foley, S. F. (2011). A Reappraisal of Redox Melting in the Earth's Mantle as a Function of Tectonic Setting and Time. *Journal of Petrology, 52*(7-8), 1363-1391. doi:10.1093/petrology/egq061

Frost, D. J., & McCammon, C. A. (2008). The redox state of Earth's mantle. *Annual Review of Earth and Planetary Sciences, 36*, 389-420. doi:10.1146/annurev.earth.36.031207.124322

Gaillard, F., Scaillet, B., Pichavant, M., & Iacono-Marziano, G. (2015). The redox geodynamics linking basalts and their mantle sources through space and time. *Chemical Geology, 418*, 217-233. doi:10.1016/j.chemgeo.2015.07.030

Gervasoni, F., Klemme, S., Rohrbach, A., Gruetzner, T., & Berndt, J. (2017). Experimental constraints on mantle metasomatism caused by silicate and carbonate melts. *Lithos, 282*, 173-186. doi:10.1016/j.lithos.2017.03.004

Ghiorso, M. S., Hirschmann, M. M., Reiners, P. W., & Kress, V. C. (2002). The pMELTS: A revision of MELTS for improved calculation of phase relations and major element partitioning related to partial melting of the mantle to 3 GPa. *Geochemistry Geophysics Geosystems, 3*. doi:10.1029/2001gc000217

Goncharov, A. G., Ionov, D. A., Doucet, L. S., & Pokhilenko, L. N. (2012). Thermal state, oxygen fugacity and C-O-H fluid speciation in cratonic lithospheric mantle: New data on peridotite xenoliths from the Udachnaya kimberlite, Siberia. *Earth and Planetary Science Letters, 357*, 99-110. doi:10.1016/j.epsl.2012.09.016

Griffin, W. L., Huang, J.-X., Thomassot, E., Gain, S. E. M., Toledo, V., & O'Reilly, S. Y. (2018). Super-reducing conditions in ancient and modern volcanic systems: sources and behaviour of carbon-rich fluids in the lithospheric mantle. *Mineralogy and Petrology, 112*, 101-114. doi:10.1007/s00710-018-0575-x

Griffin,W.L., O'Reilly, S.Y., Ryan, C.G., 1999. The composition and origin of sub-continental lithospheric mantle. In: Fei, Y., Mysen, B.O., Berltka, C.M. (Eds.), *Mantle*

Petrology: Field Observations and High-Pressure Experimentation: a Tribute to Francis R. (Joe) Boyd (pp. 13–45). Houston, TX: The Geochemical Society Special Publication.

Hao, Y.-T., Xia, Q.-K., Tian, Z.-Z., & Liu, J. (2016). Mantle metasomatism did not modify the initial H_2O content in peridotite xenoliths from the Tianchang basalts of eastern China. *Lithos, 260*, 315-327. doi:10.1016/j.lithos.2016.06.003

Hao, Y., Xia, Q., Liu, S., Feng, M., & Zhang, Y. (2012). Recognizing juvenile and relict lithospheric mantle beneath the North China Craton: Combined analysis of H_2O, major and trace elements and Sr-Nd isotope compositions of clinopyroxenes. *Lithos, 149*, 136-145. doi:10.1016/j.lithos.2012.03.013

Hong, L., Xu, Y.-G., Zhang, L., Wang, Y., & Ma, L. (2020). Recycled carbonate-induced oxidization of the convective mantle beneath Jiaodong, Eastern China. *Lithos, 366*. doi:10.1016/j.lithos.2020.105544

Ionov, D. A., Chanefo, I., & Bodinier, J. L. (2005). Origin of Fe-rich lherzolites and wehrlites from Tok, SE Siberia by reactive melt percolation in refractory mantle peridotites. *Contributions to Mineralogy and Petrology, 150*(3), 335-353. doi:10.1007/s00410-005-0026-7

Kelemen, P. B., Joyce, D. B., Webster, J. D., & Holloway, J. R. (1990). Reaction between ultramafic rock and fractionating basaltic magma .2. Experimental investigation of reaction between olivine tholeiite and harzburgite at 1150 °C-1050 °C and 5 kb. *Journal of Petrology, 31*(1), 99-134. doi:10.1093/petrology/31.1.99

Lazarov, M., Woodland, A. B., & Brey, G. P. (2009). Thermal state and redox conditions of the Kaapvaal mantle: A study of xenoliths from the Finsch mine, South Africa. *Lithos, 112*, 913-923. doi:10.1016/j.lithos.2009.03.035

Li, P., Xia, Q.-K., Deloule, E., Chen, H., Gu, X.-Y., & Feng, M. (2015). Temporal variation of H_2O content in the lithospheric mantle beneath the eastern North China Craton: Implications for the destruction of cratons. *Gondwana Research, 28*(1), 276-287. doi:10.1016/j.gr.2014.03.012

Li, S.-G., Yang, W., Ke, S., Meng, X., Tian, H., Xu, L., . . . Yan, J. (2017). Deep carbon cycles constrained by a large-scale mantle Mg isotope anomaly in eastern China. *National Science Review, 4*(1), 111-120. doi:10.1093/nsr/nww070

Liu, D. Y., Nutman, A. P., Compston, W., Wu, J. S., & Shen, Q. H. (1992). Remnants of greater-than-or-equal-to 3800 ma crust in the chinese part of the sino-korean craton. *Geology, 20*(4), 339-342. doi:10.1130/0091-7613(1992)020<0339:Romcit>2.3.Co;2

Liu, J., Rudnick, R. L., Walker, R. J., Gao, S., Wu, F.-y., Piccoli, P. M., . . . Xu, Y.-G. (2011). Mapping lithospheric boundaries using Os isotopes of mantle xenoliths: An example from the North China Craton. *Geochimica Et Cosmochimica Acta, 75*(13), 3881-3902. doi:10.1016/j.gca.2011.04.018

Luth, R. W., & Stachel, T. (2014). The buffering capacity of lithospheric mantle: implications for diamond formation. *Contributions to Mineralogy and Petrology, 168*(5). doi:10.1007/s00410-014-1083-6

Mattielli, N., Weis, D., Gregoire, M., Mennessier, J. P., Cottin, J. Y., & Giret, A. (1996). Kerguelen basic and ultrabasic xenoliths: Evidence for long-lived Kerguelen hotspot activity. *Lithos, 37*(2-3), 261-280. doi:10.1016/0024-4937(95)00040-2

Mattioli, G. S., & Wood, B. J. (1988). Magnetite activities across the $MgAl_2O_4$-Fe_3O_4 spinel join, with application to thermobarometric estimates of upper mantle oxygen fugacity. *Contributions to Mineralogy and Petrology, 98*(2), 148-162. doi:10.1007/bf00402108

McCammon, C., & Kopylova, M. G. (2004). A redox profile of the Slave mantle and oxygen fugacity control in the cratonic mantle. *Contributions to Mineralogy and Petrology, 148*(1), 55-68. doi:10.1007/s00410-004-0583-1

Menzies, M. A., & Xu, Y. G. (1998). Geodynamics of the North China Craton. In M. F. J. Flower, S. L. Chung, C. H. Lo, & T. Y. Lee (Eds.), *Mantle Dynamics and Plate Interactions in East Asia* (Vol. 27, pp. 155-165).

533 Miller, W. G. R., Holland, T. J. B., & Gibson, S. A. (2016). Garnet and Spinel
534 Oxybarometers: New Internally Consistent Multi-equilibria Models with Applications
535 to the Oxidation State of the Lithospheric Mantle. *Journal of Petrology*, 57(6), 1199-
536 1222. doi:10.1093/petrology/egw037

537 Nimis, P., & Gruetter, H. (2010). Internally consistent geothermometers for garnet
538 peridotites and pyroxenites. *Contributions to Mineralogy and Petrology, 159*(3), 411-
539 427. doi:10.1007/s00410-009-0455-9

540 Nimis, P., & Taylor, W. R. (2000). Single clinopyroxene thermobarometry for garnet
541 peridotites. Part I. Calibration and testing of a Cr-in-Cpx barometer and an enstatite-
542 in-Cpx thermometer. *Contributions to Mineralogy and Petrology, 139*(5), 541-554.
543 doi:10.1007/s004100000156

544 Norman, M. D. (1998). Melting and metasomatism in the continental lithosphere:
545 laser ablation ICPMS analysis of minerals in spinel lherzolites from eastern Australia.
546 *Contributions to Mineralogy and Petrology, 130*(3-4), 240-255.
547 doi:10.1007/s004100050363

548 O'Neill, H. S., & Wall, V. J. (1987). The Olivine-Orthopyroxene-Spinel oxygen
549 geobarometer, the nickel precipitation curve, and the oxygen fugacity of the earths
550 upper mantle. *Journal of Petrology, 28*(6), 1169-1191.
551 doi:10.1093/petrology/28.6.1169

552 Smit, K. V., Shirey, S. B., Stern, R. A., Steele, A., & Wang, W. (2016). Diamond
553 growth from C-H-N-O recycled fluids in the lithosphere: Evidence from CH_4 micro-
554 inclusions and $\delta^{13}C$-$\delta^{15}N$-N content in Marange mixed-habit diamonds. *Lithos, 265*,
555 68-81. doi:10.1016/j.lithos.2016.03.015

556 Sorbadere, F., Laurenz, V., Frost, D. J., Wenz, M., Rosenthal, A., McCammon, C., &
557 Rivard, C. (2018). The behaviour of ferric iron during partial melting of peridotite.
558 *Geochimica Et Cosmochimica Acta, 239*, 235-254. doi:10.1016/j.gca.2018.07.019

559 Stagno, V., Ojwang, D. O., McCammon, C. A., & Frost, D. J. (2013). The oxidation
560 state of the mantle and the extraction of carbon from Earth's interior. *Nature,*

493(7430), 84-+. doi:10.1038/nature11679

Sun, C., & Dasgupta, R. (2020). Thermobarometry of CO_2-rich, silica-undersaturated melts constrains cratonic lithosphere thinning through time in areas of kimberlitic magmatism. *Earth and Planetary Science Letters, 550*. doi:10.1016/j.epsl.2020.116549

Tang, Y.-J., Zhang, H.-F., Ying, J.-F., Zhang, J., & Liu, X.-M. (2008). Refertilization of ancient lithospheric mantle beneath the central North China Craton: Evidence from petrology and geochemistry of peridotite xenoliths. *Lithos, 101*(3-4), 435-452. doi:10.1016/j.lithos.2007.09.006

Taylor, W. R. (1998). An experimental test of some geothermometer and geobarometer formulations for upper mantle peridotites with application to the thermobarometry of fertile lherzolite and garnet websterite. *Neues Jahrbuch Fur Mineralogie-Abhandlungen, 172*(2-3), 381-408. Retrieved from <Go to ISI>://WOS:000073997000016

Thomassot, E., Cartigny, P., Harris, J. W., & Viljoen, K. S. (2007). Methane-related diamond crystallization in the Earth's mantle: Stable isotope evidences from a single diamond-bearing xenolith. *Earth and Planetary Science Letters, 257*(3-4), 362-371. doi:10.1016/j.epsl.2007.02.020

Till, C. B., Grove, T. L., & Krawczynski, M. J. (2012). A melting model for variably depleted and enriched lherzolite in the plagioclase and spinel stability fields. *Journal of Geophysical Research-Solid Earth, 117*. doi:10.1029/2011jb009044

Wang, Q., Bagdassarov, N., Xia, Q.-K., & Zhu, B. (2014). Water contents and electrical conductivity of peridotite xenoliths from the North China Craton: Implications for water distribution in the upper mantle. *Lithos, 189*, 105-126. doi:10.1016/j.lithos.2013.08.005

Woodland, A. B., & Koch, M. (2003). Variation in oxygen fugacity with depth in the upper mantle beneath the Kaapvaal craton, Southern Africa. *Earth and Planetary Science Letters, 214*(1-2), 295-310. doi:10.1016/s0012-821x(03)00379-0

589 Woodland, A. B., Kornprobst, J., & Tabit, A. (2006). Ferric iron in orogenic lherzolite
590 massifs and controls of oxygen fugacity in the upper mantle. *Lithos, 89*(1-2), 222-241.
591 doi:10.1016/j.lithos.2005.12.014

592 Workman, R. K., & Hart, S. R. (2005). Major and trace element composition of the
593 depleted MORB mantle (DMM). *Earth and Planetary Science Letters, 231*(1-2), 53-
594 72. doi:10.1016/j.epsl.2004.12.005

595 Wu, D., Liu, Y., Chen, C., Xu, R., Ducea, M. N., Hu, Z., & Zong, K. (2017). In-situ
596 trace element and Sr isotopic compositions of mantle xenoliths constrain two-stage
597 metasomatism beneath the northern North China Craton. *Lithos, 288*, 338-351.
598 doi:10.1016/j.lithos.2017.07.018

599 Wu, F.-Y., Yang, J.-H., Xu, Y.-G., Wilde, S. A., & Walker, R. J. (2019). Destruction of
600 the North China Craton in the Mesozoic. In R. Jeanloz & K. H. Freeman (Eds.),
601 *Annual Review of Earth and Planetary Sciences, Vol 47* (Vol. 47, pp. 173-+).

602 Xia, Q.-K., Hao, Y.-T., Liu, S.-C., Gu, X.-Y., & Feng, M. (2013). Water contents of
603 the Cenozoic lithospheric mantle beneath the western part of the North China Craton:
604 Peridotite xenolith constraints. *Gondwana Research, 23*(1), 108-118.
605 doi:10.1016/j.gr.2012.01.010

606 Xia, Q.-K., Hao, Y., Li, P., Deloule, E., Coltorti, M., Dallai, L., . . . Feng, M. (2010).
607 Low water content of the Cenozoic lithospheric mantle beneath the eastern part of the
608 North China Craton. *Journal of Geophysical Research-Solid Earth, 115*.
609 doi:10.1029/2009jb006694

610 Xiao, Y., Zhang, H.-F., Fan, W.-M., Ying, J.-F., Zhang, J., Zhao, X.-M., & Su, B.-X.
611 (2010). Evolution of lithospheric mantle beneath the Tan-Lu fault zone, eastern North
612 China Craton: Evidence from petrology and geochemistry of peridotite xenoliths.
613 *Lithos, 117*(1-4), 229-246. doi:10.1016/j.lithos.2010.02.017

614 Xu, W., Yang, D., Gao, S., Pei, F., & Yu, Y. (2010). Geochemistry of peridotite
615 xenoliths in Early Cretaceous high-Mg# diorites from the Central Orogenic Block of
616 the North China Craton: The nature of Mesozoic lithospheric mantle and constraints

on lithospheric thinning. *Chemical Geology, 270*(1-4), 257-273. doi:10.1016/j.chemgeo.2009.12.006

Xu, Y., Li, H., Hong, L., Ma, L., Ma, Q., & Sun, M. (2018). Generation of Cenozoic intraplate basalts in the big mantle wedge under eastern Asia. *Science China-Earth Sciences, 61*(7), 869-886. doi:10.1007/s11430-017-9192-y

Yang, X.-Z., Xia, Q.-K., Deloule, E., Dallai, L., Fan, Q.-C., & Feng, M. (2008). Water in minerals of the continental lithospheric mantle and overlying lower crust: A comparative study of peridotite and granulite xenoliths from the North China Craton. *Chemical Geology, 256*(1-2), 33-45. doi:10.1016/j.chemgeo.2008.07.020

Yaxley, G. M., Berry, A. J., Kamenetsky, V. S., Woodland, A. B., & Golovin, A. V. (2012). An oxygen fugacity profile through the Siberian Craton - Fe K-edge XANES determinations of $Fe^{3+}/\Sigma Fe$ in garnets in peridotite xenoliths from the Udachnaya East kimberlite. *Lithos, 140*, 142-151. doi:10.1016/j.lithos.2012.01.016

Ying, J. F., Zhang, H. F., Kita, N., Morishita, Y., & Shimoda, G. (2006). Nature and evolution of late cretaceous lithospheric mantle beneath the eastern North China Craton: Constraints from petrology and geochemistry of peridotitic xenoliths from Junan, Shandong Province, China. *Earth and Planetary Science Letters, 244*(3-4), 622-638. doi:10.1016/j.epsl.2006.02.023

Zhang, C., & Duan, Z. (2009). A model for C-O-H fluid in the Earth's mantle. *Geochimica Et Cosmochimica Acta, 73*(7), 2089-2102. doi:10.1016/j.gca.2009.01.021

Zhang, C., & Duan, Z. (2010). GFluid: An Excel spreadsheet for investigating C-O-H fluid composition under high temperatures and pressures. *Computers & Geosciences, 36*(4), 569-572. doi:10.1016/j.cageo.2009.05.008

Zhang, H.-F., Nakamura, E., Sun, M., Kobayashi, K., Zhang, J., Ying, J.-F., . . . Niu, L.-F. (2007). Transformation of subcontinental lithospheric mantle through peridotite-melt reaction: Evidence from a highly fertile mantle xenolith from the north China Craton. *International Geology Review, 49*(7), 658-679. doi:10.2747/0020-6814.49.7.658

Zhao, G. C., Sun, M., Wilde, S. A., & Li, S. Z. (2005). Late Archean to Paleoproterozoic evolution of the North China Craton: key issues revisited. *Precambrian Research, 136*(2), 177-202. doi:10.1016/j.precamres.2004.10.002

Zheng, J., Griffin, W. L., O'Reilly, S. Y., Yang, J., Li, T., Zhang, M., . . . Liou, J. G. (2006). Mineral chemistry of peridotites from Paleozoic, Mesozoic and Cenozoic lithosphere: Constraints on mantle evolution beneath eastern China. *Journal of Petrology, 47*(11), 2233-2256. doi:10.1093/petrology/egl042

Zheng, J. P., Griffin, W. L., Ma, Q., O'Reilly, S. Y., Xiong, Q., Tang, H. Y., . . . Su, Y. P. (2012). Accretion and reworking beneath the North China Craton. *Lithos, 149*, 61-78. doi:10.1016/j.lithos.2012.04.025

Zheng, J. P., O'Reilly, S. Y., Griffin, W. L., Lu, F. X., Zhang, M., & Pearson, N. J. (2001). Relict refractory mantle beneath the eastern North China block: significance for lithosphere evolution. *Lithos, 57*(1), 43-66. doi:10.1016/s0024-4937(00)00073-6

Zheng, Y., Xu, Z., Zhao, Z., & Dai, L. (2018). Mesozoic mafic magmatism in North China: Implications for thinning and destruction of cratonic lithosphere. *Science China-Earth Sciences, 61*(4), 353-385. doi:10.1007/s11430-017-9160-3

Ziberna, L., Klemme, S., & Nimis, P. (2013). Garnet and spinel in fertile and depleted mantle: insights from thermodynamic modelling. *Contributions to Mineralogy and Petrology, 166*(2), 411-421. doi:10.1007/s00410-013-0882-5

References From the Supporting Information

Chen, J. C., Hsu, C. N., & Ho, K. S. (2003). Geochemistry of Cenozoic volcanic rocks and related ultramafic xenoliths from the Jilin and Heilongjiang provinces, northeast China. *Journal of Asian Earth Sciences, 21*(9), 1069-1084. doi:10.1016/s1367-9120(02)00144-x

Chen, S. H., O'Reilly, S. Y., Zhou, X. H., Griffin, W. L., Zhang, G. H., Sun, M., . . . Zhang, M. (2001). Thermal and petrological structure of the lithosphere beneath Hannuoba, Sino-Korean Craton, China: evidence from xenoliths. *Lithos, 56*(4), 267-301. doi:10.1016/s0024-4937(00)00065-7

Chu, Z.-Y., Wu, F.-Y., Walker, R. J., Rudnick, R. L., Pitcher, L., Puchtel, I. S., . . . Wilde, S. A. (2009). Temporal Evolution of the Lithospheric Mantle beneath the Eastern North China Craton. *Journal of Petrology, 50*(10), 1857-1898. doi:10.1093/petrology/egp055

Deng, L., Liu, Y., Zong, K., Zhu, L., Xu, R., Hu, Z., & Gao, S. (2017). Trace element and Sr isotope records of multi-episode carbonatite metasomatism on the eastern margin of the North China Craton. *Geochemistry Geophysics Geosystems, 18*(1), 220-237. doi:10.1002/2016gc006618

Hong, L.-B., Xu, Y.-G., Ren, Z.-Y., Kuang, Y.-S., Zhang, Y.-L., Li, J., . . . Zhang, H. (2012). Petrology, geochemistry and Re-Os isotopes of peridotite xenoliths from Yantai, Shandong Province: Evidence for Phanerozoic lithospheric mantle beneath eastern North China Craton. *Lithos, 155*, 256-271. doi:10.1016/j.lithos.2012.09.005

Hu, Y., Teng, F.-Z., Zhang, H.-F., Xiao, Y., & Su, B.-X. (2016). Metasomatism-induced mantle magnesium isotopic heterogeneity: Evidence from pyroxenites. *Geochimica Et Cosmochimica Acta, 185*, 88-111. doi:10.1016/j.gca.2015.11.001

Liu, J., Carlson, R. W., Rudnick, R. L., Walker, R. J., Gao, S., & Wu, F.-Y. (2012). Comparative Sr-Nd-Hf-Os-Pb isotope systematics of xenolithic peridotites from Yangyuan, North China Craton: Additional evidence for a Paleoproterozoic age. *Chemical Geology*, 332, 1-14. doi:10.1016/j.chemgeo.2012.09.013

Rudnick, R. L., Shan, G., Ling, W. L., Liu, Y. S., & McDonough, W. F. (2004). Petrology and geochemistry of spinel peridotite xenoliths from Hannuoba and Qixia, North China Craton. *Lithos, 77*(1-4), 609-637. doi:10.1016/j.lithos.2004.03.033

Tang, Y.-J., Zhang, H.-F., Deloule, E., Su, B.-X., Ying, J.-F., Xiao, Y., & Hu, Y. (2012). Slab-derived lithium isotopic signatures in mantle xenoliths from northeastern North China Craton. *Lithos, 149*, 79-90. doi:10.1016/j.lithos.2011.12.001

Tang, Y.-J., Zhang, H.-F., Nakamura, E., Moriguti, T., Kobayashi, K., & Ying, J.-F. (2007). Lithium isotopic systematics of peridotite xenoliths from Hannuoba, North China Craton: Implications for melt-rock interaction in the considerably thinned lithospheric mantle. *Geochimica Et Cosmochimica Acta, 71*(17), 4327-4341. doi:10.1016/j.gca.2007.07.006

Wang, C., Liu, Y., Foley, S. F., Zong, K., & Hu, Z. (2019). Lithospheric transformation of the northern North China Craton by changing subduction style of the Paleo-Asian oceanic plate: Constraints from peridotite and pyroxenite xenoliths in the Yangyuan basalts. *Lithos, 328*, 58-68. doi:10.1016/j.lithos.2019.01.018

Wu, F.-Y., Walker, R. J., Yang, Y.-H., Yuan, H.-L., & Yang, J.-H. (2006). The chemical-temporal evolution of lithospheric mantle underlying the North China Craton. *Geochimica Et Cosmochimica Acta, 70*(19), 5013-5034. doi:10.1016/j.gca.2006.07.014

Xu, Q., Liu, J., He, H., & Zhang, Y. (2019). Nature and evolution of the lithospheric mantle revealed by water contents and He-Ar isotopes of peridotite xenoliths from Changbaishan and Longgang basalts in Northeast China. *Science Bulletin, 64*(18), 1325-1335. doi:10.1016/j.scib.2019.07.006

Xu, Y. G., & Bodinier, J. L. (2004). Contrasting enrichments in high- and low-temperature mantle xenoliths from Nushan, eastern China: Results of a single metasomatic event during lithospheric accretion? *Journal of Petrology, 45*(2), 321-341. doi:10.1093/petrology/egg098

Yang, J.-H., Zhang, M., & Wu, F.-Y. (2018). Mesozoic decratonization of the North China Craton by lithospheric delamination: Evidence from Sr-Nd-Hf-Os isotopes of mantle xenoliths of Cenozoic alkaline basalts in Yangyuan, Hebei Province, China. *Journal of Asian Earth Sciences, 160*, 396-407. doi:10.1016/j.jseaes.2017.09.002

Zhang, J., Zhang, H., Kita, N., Shimoda, G., Morishita, Y., Ying, J., & Tang, Y. (2011). Secular evolution of the lithospheric mantle beneath the eastern North China craton: evidence from peridotitic xenoliths from Late Cretaceous mafic rocks in the Jiaodong region, east-central China. *International Geology Review, 53*(2), 182-211. doi:10.1080/00206810903025090

722 Zhao, X.-M., Zhang, H.-F., Zhu, X.-K., Zhu, B., & Cao, H.-h. (2015). Effects of melt percolation
723 on iron isotopic variation in peridotites from Yangyuan, North China Craton. *Chemical Geology,*
724 *401*, 96-110. doi:10.1016/j.chemgeo.2015.02.031

725 Zhao, X., Wang, H., Li, Z., Liu, F., Evans, N. J., & Zhang, H. (2020). Multi-stage metasomatism
726 of lithospheric mantle by asthenosphere-derived melts: evidence from mantle xenoliths in
727 daxizhuang at the eastern North China craton. *Mineralogy and Petrology, 114*(2), 141-159.
728 doi:10.1007/s00710-020-00697-w

729 Zhao, X., Zhang, H., Zhu, X., Tang, S., & Tang, Y. (2010). Iron isotope variations in spinel
730 peridotite xenoliths from North China Craton: implications for mantle metasomatism.
731 *Contributions to Mineralogy and Petrology, 160*(1), 1-14. doi:10.1007/s00410-009-0461-y

732 Zheng, J., Griffin, W. L., O'Reilly, S. Y., Yang, J., Li, T., Zhang, M., . . . Liou, J. G. (2006).
733 Mineral chemistry of peridotites from Paleozoic, Mesozoic and Cenozoic lithosphere:
734 Constraints on mantle evolution beneath eastern China. Journal of Petrology, 47(11), 2233-2256.
735 doi:10.1093/petrology/egl042

736 Zheng, J. P., Griffin, W. L., O'Reilly, S. Y., Yu, C. M., Zhang, H. F., Pearson, N., & Zhang, M.
737 (2007). Mechanism and timing of lithospheric modification and replacement beneath the eastern
738 North China Craton: Peridotitic xenoliths from the 100 Ma Fuxin basalts and a regional
739 synthesis. *Geochimica Et Cosmochimica Acta, 71*(21), 5203-5225.
740 doi:10.1016/j.gca.2007.07.028

741 Zheng, J. P., O'Reilly, S. Y., Griffin, W. L., Lu, F. X., & Zhang, M. (1998). Nature and evolution
742 of Cenozoic lithospheric mantle beneath Shandong peninsula, Sino-Korean craton, eastern
743 China. *International Geology Review, 40*(6), 471-499. doi:10.1080/00206819809465220

744 Zou, D., Zhang, H., Hu, Z., & Santosh, M. (2016). Complex metasomatism of lithospheric
745 mantle by asthenosphere-derived melts: Evidence from peridotite xenoliths in Weichang at the
746 northern margin of the North China Craton. *Lithos, 264*, 210-223.
747 doi:10.1016/j.lithos.2016.08.036

748 Zou, D., Zhang, H., Zhang, X., Zhang, H., & Su, B. (2020). Refertilization of lithospheric mantle
749 beneath the North China Craton in Mesozoic: Evidence from in situ Sr isotopes of Fuxin
750 peridotite. *Lithos, 364*. doi:10.1016/j.lithos.2020.10547